Title

Cytoplasmic Flow and Mixing Due to Deformation of Motile Cells.

Journal

Biophysical Journal, 113(9)

Authors

Chan, Caleb

Theriot, Julie

Koslover, Elena

Publication Date

2017-11-07

DOI

10.1016/j.bpj.2017.09.009

Peer reviewed

Biophysical Journal
Article

Biophysical Society

Cytoplasmic Flow and Mixing Due to Deformation of Motile Cells

Elena F. Koslover,[1,*] Caleb K. Chan,[2] and Julie A. Theriot[2,3,4]
[1]Department of Physics, University of California, San Diego, San Diego, California; [2]Department of Biochemistry, [3]Department of Microbiology and Immunology, and [4]Howard Hughes Medical Institute, Stanford University School of Medicine, Stanford, California

ABSTRACT The cytoplasm of a living cell is a dynamic environment through which intracellular components must move and mix. In motile, rapidly deforming cells such as human neutrophils, bulk cytoplasmic flow couples cell deformation to the transport and dispersion of cytoplasmic particles. Using particle-tracking measurements in live neutrophil-like cells, we demonstrate that fluid flow associated with the cell deformation contributes to the motion of small acidic organelles, dominating over diffusion on timescales above a few seconds. We then use a general physical model of particle dispersion in a deforming fluid domain to show that transport of organelle-sized particles between the cell periphery and the bulk can be enhanced by dynamic deformation comparable to that observed in neutrophils. Our results implicate an important mechanism contributing to organelle transport in these motile cells: cytoplasmic flow driven by cell shape deformation.

INTRODUCTION

Eukaryotic cells must be able to transport cellular components ranging from small molecules to micron-sized organelles, across distances that span from tens of microns in compact cells to centimeters in neuronal axons. The most well-known mechanisms of transport are passive diffusion, which can spread small particles over short distances, and active transport by motor proteins walking along cytoskeletal filaments, which can move cargo in a directed fashion at rates up to 2 μm/s (1). Additional motion stems from dispersed active fluctuations in the living cytoplasm (2,3), which can substantially enhance the apparently diffusive movements of organelle-sized particles (4–6).

Another mode of transport through the cytoplasm is advection due to flow of the cytoplasmic fluid. This flow can arise from hydrodynamic entrainment by concerted motion of motor proteins, as has been observed in the cytoplasmic streaming of plant cells, which can reach rates of 50 μm/s (7), as well as the slower cytoplasmic flows of fly, nematode, and mouse oocytes (8,9). In motile cells such as keratocytes, hydrostatic pressures generated by myosin-driven cytoskeletal contraction lead to cytoplasmic flows on the order of 0.1 μm/s, which are believed to contribute to the transport of crucial molecular components toward the leading edge (10). Yet another potential source of flow comes from the deformation of the cell itself. Large pulsatile flows have been observed within contracting embryonic cells (11) and in the slime mold *Physarum polycephalum*, where fluid flow is driven by peristaltic contraction in amoeboid-like fragments (12) and expansive tubular networks (13). Many other motile cell types, such as amoebas (14), fibroblasts (15), and leukocytes (16), also exhibit substantial changes in cell shape, albeit without the characteristic periodicity associated with organized peristalsis. Yet another canonical mode of shape change in animal cells is associated with blebbing, the formation of bubble-like structures where the membrane peels away from the cytoskeletal cortex (17). The dynamics of such blebs, which occur during cell migration in a three-dimensional environment (18) and at the advent of apoptosis (19), are determined by the flow of the cytoplasmic fluid and its interaction with the cytoskeletal network (17,20,21).

In this work, we explore the effect of flows associated with cell deformation on particle transport throughout the cytoplasm of a moving cell, focusing specifically on motile, neutrophil-like HL60 cells, which deform substantially on minute-long timescales while crawling in a two-dimensional environment. In the human body, neutrophil cells move through a three-dimensional matrix, and are also believed to undergo large shape deformations as they extravasate into tissues and engulf pathogens. These cells are actively phagocytic and contain large numbers of

Submitted April 10, 2017, and accepted for publication September 11, 2017.
*Correspondence: ekoslover@physics.ucsd.edu
Editor: Cecile Sykes.
https://doi.org/10.1016/j.bpj.2017.09.009

granules that release antimicrobial compounds. Their ability to transport vesicles and granules between the cell center and the periphery is thus crucial to their immunological function.

The effect of cell shape deformation on the motion of its cytoplasmic contents is inextricably dependent on the coarse material properties of the cytoplasm itself. In the case of a purely elastic cytoplasm, the cell would maintain a consistent internal coordinate system that deforms together with its boundary, leading to no net motion of the contents once it returns to its original shape. Microscopically, this behavior would arise if the cell deformation merely compressed and stretched an internal cytoskeletal network without large-scale rearrangements. In the case of a viscous or viscoelastic cytoplasmic fluid, however, nonreciprocal deformations of the cell would lead to a net displacement of cytoplasmic contents even if the original shape is restored. Such a rheology would arise from cytoskeletal remodeling and turnover on timescales sufficiently rapid compared with the overall deformation of the cell.

There has been much recent debate in the literature concerning the rheology of the eukaryotic cytoplasm (22,23). Passive particle tracking in stationary cells has indicated diffusive motion in some cases, as in a viscous medium (24,25), and subdiffusion in other cases, as expected for a viscoelastic environment (26–29). Even where intracellular particles appear to move diffusively, it has been shown that their stochastic motion is strongly dependent on active processes dispersed throughout the cytoplasm (2,5,6,30–32). Coupled active and passive microrheology studies in living cells give rise to a picture of the cytoplasm as primarily elastic on timescales below $\sim$10 s, with organelle-sized particles nonetheless exhibiting apparently diffusive motion driven by the accumulation of spatially uncorrelated active forces that are processive on the multisecond timescale (5,33–35). At much longer times, however, we would expect an upper limit on the relaxation times for stresses within the cytoplasm, allowing viscous deformation of the cell and long-range movement of its organelles without elastic restoring forces driving the cytoplasm to its original morphology. This expectation underlies many prior studies modeling cell mechanics (36–39) and is justified by the fact that the actin cytoskeleton, which is thought to endow the cell with its elastic properties, has a turnover time on the order of 20 s (40,41). The notion of a viscous cytoplasm at long times is consistent with bulk rheology data, which demonstrates that highly deformable cells such as neutrophils behave effectively as fluid droplets in pipette aspiration experiments (42).

In this study, we focus on the role of cytoplasmic flow associated with cell deformation, which proceeds on a timescale of multiple minutes. In our analysis, we make the simplifying assumption of treating the cytoplasm of neutrophil-like cells as a purely viscous fluid over all times. In practice, this can be broken down into two consequential assumptions. First, we assume that the stochastic Brownian motion of organelles in the cytoplasm is diffusive, as evidenced by prior data on organelle trajectories in neutrophil-like cells (43) and other motile cell types (25). Whether this stochastic motion arises from thermal noise or from uncorrelated active forces scattered throughout the cytoplasm, we treat it simply as a diffusive process with a known effective diffusion coefficient. Second, our calculations of the cytoplasmic flows associated with deforming cell shape assume the bulk rheology of the cytoplasm to be that of a viscous fluid. This assumption is justified on the minute timescales by pipette aspiration experiments, and is extended to all times for purposes of simplification and given the lack of detailed rheology data on the transition between an elastic and a viscous cytoplasm at intermediate times. Our focus in this work is on determining the relative contributions of the effectively diffusive motion and the deformation-driven flow to the transport of organelles within motile cells.

For deforming a viscous domain, two effects combine to contribute toward the mixing of passive particles within the cell: diffusion that smears out local concentration fluctuations, and Lagrangian stirring (the chaotic motion of particles driven by a spatially heterogeneous unsteady flow) (44,45). Differential rates of flow within the cytoplasm can additionally increase particle diffusivity through Taylor dispersion, an effect where shear flow enhances diffusive spreading by stretching out concentrated clusters of particles. Lagrangian chaos and Taylor dispersion have been previously characterized for simple oscillatory fluid flows (46–48). Additionally, the Taylor dispersion resulting from traveling waves in a contracting network of tubes has been studied in the context of flows within *P. polycephalum* slime molds, where this effect was found to be essential for long-distance transport of nutrients within the organism (13). However, the magnitude of such fluid dynamic effects for the particular case of a flow generated by a randomly deforming compact domain, for size and timescales relevant to motile amoeboid cells, has not, to the best of our knowledge, been previously characterized.

We use in vivo tracking of endogenous organelles within crawling HL60 cells, together with computation of expected fluid flows associated with cell deformation, to demonstrate that such flows both correlate with organelle motion and are expected to dominate over diffusion on biologically relevant time and spatial scales. We then develop a minimalist model of a deforming fluid domain to explore the more general physical question of how deformation-driven flow affects the mixing of embedded particles and their transport between different regions of the cell. Our calculations demonstrate that, for parameter values relevant to organelle motion in motile cells, modest deformations of the fluid domain can enhance the rate at which particles move between the domain center and the periphery.

MATERIALS AND METHODS

Organelle tracking in HL60 cells

Motile, neutrophil-like HL60 cells were differentiated according to a standard protocol, labeled with fluorescent lysotracker dye, and imaged at 20 Hz in a two-dimensional under-agarose environment, at uniform chemoattractant concentrations, using a Nikon Eclipse Ti epifluorescence microscope with a 100× oil-immersion objective, employing the same equipment and procedure as was described in our previous work (43). Individual organelle trajectories were exacted from a total of 78 cells according to a standard particle-tracking procedure (43,49,50). A median of 338 trajectories with median length 4.5 s were extracted from each cell. A sample movie of a cell used for extracting lysotracker trajectories is provided in Movie S1.

For computing one- and two-particle velocity correlation functions (50), the particle trajectories were calculated in the cell frame of reference. The cell frame of reference was found by cross correlating raw fluorescent image data for each cell between every 10th frame of the fluorescent images (time intervals of 0.5 s) (51). The translational displacement of a rectangular region around the cell that yielded the highest cross correlation with the previous image was taken as an approximation for the shift in the cell frame of reference between the images. These shifts were integrated forward to determine the position of the cell frame of reference over time. The cell frame does not account for any rotation of the cells, which generally do not exhibit rigid body rotations over half-second time intervals.

Additionally, we robustly account for the overall translational and rotational motion of the cell by reporting the time- and ensemble-averaged, mean-squared displacement (MSD) of interparticle distances (defined in Supporting Materials and Methods, *Statistical metrics for lysosome motion in HL60 cells*), calculated among all pairs of trajectories in each individual cell (52,53). Details of the statistical measures reported in Fig. 1 are described in Supporting Materials and Methods, *Statistical metrics for lysosome motion in HL60 cells*.

Fluid flow from cell deformation

To accurately determine cell shape deformation over time, four HL60 cells, prepared as described previously, were additionally subjected to short periodic overlay of phase-contrast and fluorescence channels at 4 s (80 frame) intervals. The cell contour was extracted from these phase-contrast images using the directional gradient vector flow algorithm (54).

Contours were aligned to maintain coincidence of tail projection regions and thereby avoid rotation around the contour, and were interpolated over time with splines. Comparison of independently segmented contours in consecutive phase frames (0.05 s separation) indicated a root MSD of 0.2 μm between aligned contour points, which we take as an approximate measure for the segmentation accuracy. The root mean-squared velocity of contour points relative to the cell center of mass was 0.2 μm/s, so that the boundary motion over the 4 s time intervals between segmented frames is expected to substantially exceed the segmentation error. An example movie showing the traced cell contour superimposed on phase-contrast and fluorescent lysotracker images is provided in Movie S2.

The extracted contour velocities were then used as a boundary condition for two-dimensional, finite element simulations of the internal fluid flow, using the software COMSOL Multiphysics. Lagrangian trajectories of simulated point particles were tracked within the calculated fluid flow at 0.5 s intervals. For correlation with observed lysosome motion (Fig. 2 *c*), measured velocities of (on average) 340 acidified particles per cell were temporally smoothed with a 30-frame (1.5 s) Savitsky-Golay filter, and spatially smoothed with a Gaussian filter with $\sigma = 1.5$ μm. The correlation

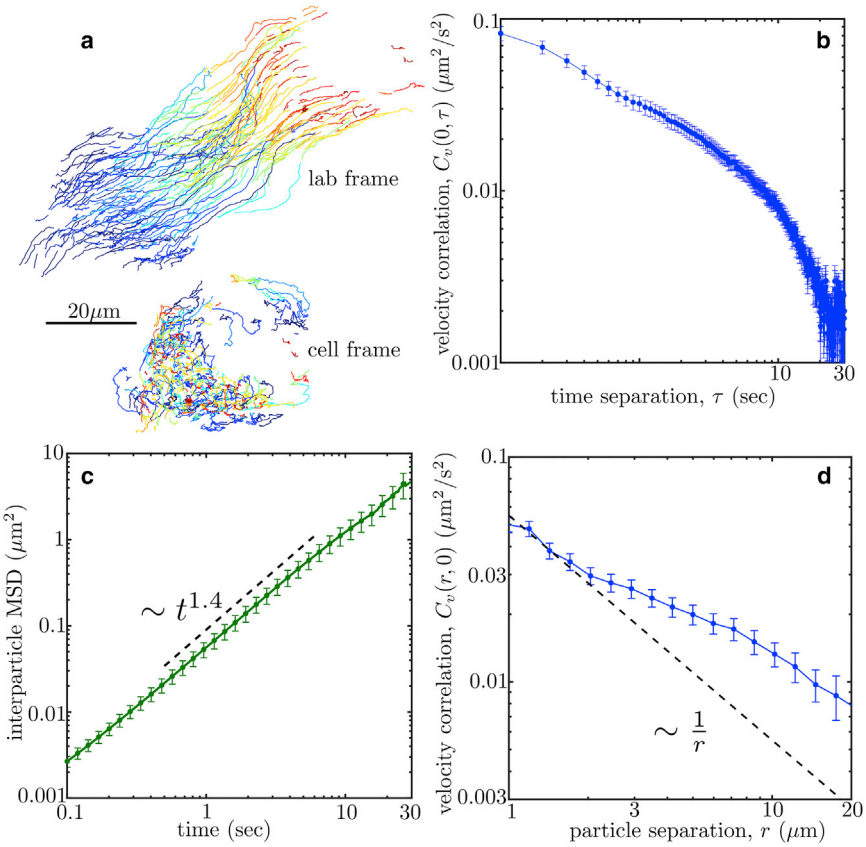

FIGURE 1 Lysosome motion in motile HL60 cells is correlated in space and time. (*a*) Lysosomal particle trajectories for an example cell, tracked over 90 s, shown in the laboratory frame of reference (*top*) and the cell frame of reference (*bottom*). (*b*) Velocity autocorrelation function (relative to cell frame), averaged over time and cell ensemble, indicating persistently correlated particle velocities. (*c*) Time- and ensemble-averaged MSD of interparticle distances, showing superdiffusive scaling. (*d*) Time- and ensemble-averaged cross correlation of particle velocities (relative to cell frame), as a function of separation between particles. Dashed line shows $1/r$ scaling expected for a quiescent continuous medium (50). Error bars in (*b*)–(*d*) correspond to standard error of the mean, assuming measurements from individual cells to be independent. To see this figure in color, go online.

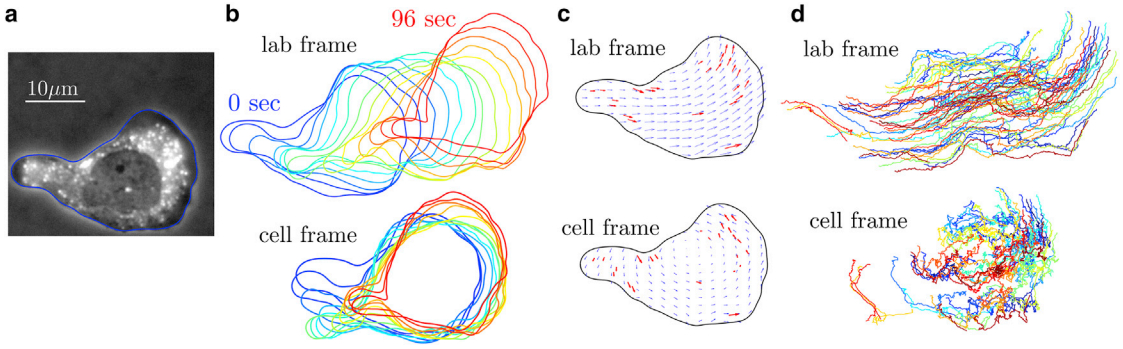

FIGURE 2 Simulation of fluid flow driven by deforming boundary of HL60 cells. (*a*) Phase-contrast image together with lysotracker fluorescence in an example cell, overlayed by cell contour outline (*blue*). (*b*) Colored contours show outline of the cell tracked over 96 s, in the laboratory frame of reference (*top*) and the cell frame of reference (*bottom*). (*c*) Snapshots of two-dimensional fluid flow solution using cell contour motion as a boundary condition. Blue arrows show the calculated velocity field. Red arrows indicate time- and space-smoothed velocities of tracked lysosomal particles. (*d*) Example trajectories for simulated particles undergoing diffusion on top of the calculated fluid flow. To see this figure in color, go online.

between these smoothed velocities and simulated results was defined as $\langle \vec{v}_{\rm sim}(\vec{x}_i)\cdot\vec{v}_i\rangle/\sqrt{\langle \vec{v}_{\rm sim}^2(\vec{x}_i)\rangle\langle \vec{v}_i^2\rangle}$, where $\vec{x}_i$, $\vec{v}_i$ represent the positions and smoothed velocities of individual lysosomes in the cell, $\vec{v}_{\rm sim}$ is the simulated velocity based on boundary deformation, and averages are done over all particles, i, for all snapshots separated by 0.5 s time intervals, for a given cell.

Computational model of deforming domain

To address the role of deformation-driven flow on long-time particle mixing, we developed an abstract, highly simplified model of particle motion in a deforming fluid domain. A spectral boundary integral method was used to solve for the fluid flow associated with the deformation (elongation along a varying axis) of a quasi-spherical domain (of undeformed radius R_0), as described in detail in Supporting Materials and Methods, *Simulating flow in a deforming domain with the spectral boundary integral method*. Briefly, a lowest-mode deformation, corresponding to domain elongation, proceeds periodically to a relative magnitude of 0.8, along an axis that is selected randomly at the start of each elongation period. That axis then rotates at a constant velocity in an arbitrarily chosen direction over the course of the deformation cycle.

Lagrangian trajectories for 1000–4000 particles driven by diffusion and flow are tracked in each simulation, using a forward time-stepping algorithm, until they come within an absorbing distance of $0.02R_0$ of either the domain periphery or a central solid region of size $0.4R_0$, representing the nucleus. For each parameter set, 10 replicates of the simulations are carried out, averaging over different trajectories of the deformation axis. Curves of the distribution of absorbed particles over time (Fig. 5, *a* and *c*) are fitted to analytical solutions for encounter rates to an absorbing boundary in two or three dimensions, in an undeformed spherical domain (see Supporting Materials and Methods, *Fitting D_{eff} for boundary encounter rates*).

We describe the enhancement in particle absorption due to domain deformation for a wide range of parameter values, to illustrate the dependence on the relative rates of the dynamic deformation and particle diffusion. The appropriate values for the deformation period and rate of axis rotation in motile neutrophils are approximated from low-resolution, long-time trajectories of whole neutrophil cells, as described in Supporting Materials and Methods, *Parameter estimation from HL60 trajectory statistics*. Whole-cell trajectories for these approximations were extracted from movie footage of DAPI-stained cell nuclei, gathered at 15× magnification with a frame rate of 0.1 Hz, using the same imaging equipment as for the organelle tracking (see Movie S3).

RESULTS AND DISCUSSION

Particle motion in motile neutrophils

To explore the role of deformation-driven flow in particle transport and mixing within a specific cellular system, we studied the motion of acidified organelles (including lysosomes and granules) in the cytoplasm of motile, neutrophil-like HL60 cells. For ease of imaging, cells were confined to a two-dimensional environment, where they spontaneously polarized and crawled under a uniform field of chemoattractant (43). We used a fluorescent lysotracker dye to label discrete acidified organelles, which for simplicity we will refer to as lysosomes, and tracked them over the course of the cells' movement (Fig. 1 *a*).

These particles exhibit positively correlated velocities (Fig. 1 *b*) over 10 s that indicate directionally persistent movement, rather than the random steps associated with Brownian motion. To isolate the relative motion of particles within the cell from overall cell translation and rotation, we calculated interparticle distances for all pairs of particles and tracked their variation over time. The MSD of interparticle distances scales superlinearly with time (Fig. 1 *c*), implying that the particles move superdiffusively within the cytoplasm, in agreement with prior results for particle motion in deforming amoeboid cells (14).

Our previous work has indicated that the movement of lysosomes in neutrophils can be decomposed into a persistent component that is highly correlated in time, superimposed with an effectively diffusive motion (43). Analysis of spatial correlations demonstrates that lysosome velocities remain correlated across length scales comparable with the size of the cell, even when the overall translational motion of the cell is removed (Fig. 1 *d*). Such correlated particle movement is unlikely to be caused by active motor-driven transport along cytoskeletal highways, a mechanism which has previously been shown to result in superdiffusive scaling of particle MSD (55). Specifically, the bidirectional nature

of motor-driven lysosome transport (56,57) should yield no net correlation between the velocities of spatially separated lysosomes, even if they move along orientationally aligned microtubules. The persistence of spatial correlations over 10 microns argues for a substantial component of the vesicle motion arising from dynamics on a whole-cell scale. We propose that this motion is associated with advective flow arising from the deformation of the cell itself.

To quantify the expected motion of particles due to the deformation of the crawling cell, we reduced the cell to a simplified model system. First, we treated the cytoplasm as a viscous fluid on the relevant timescales, with organelle motion driven by an effective diffusion together with fluid flow, as discussed in the Introduction. The viscous fluid is assumed to undergo creeping flow, as is appropriate for cellular systems with a very low Reynolds number (58). Additionally, we approximated the cytoplasmic flow as two-dimensional, an assumption that is justified by prior data demonstrating that the top and bottom surface of leukocyte and keratocyte cells move in concert, and no "tank-treading" motion is observed in these cell types (59,60). The outline of the HL60 cells was tracked from periodic phase-contrast microscopy images taken every 4 s (Fig. 2, *a* and *b*; Movie S2). The area enclosed by the tracked outline remained approximately constant over time, with the square root of the area for each cell exhibiting a root mean-square deviation of 0.1 μm, well within the estimated error of boundary tracking (see Materials and Methods). The maintenance of a constant area within the cell enables us to model the enclosed cytoplasm as a two-dimensional incompressible fluid. The outline motion was used as a fixed-velocity boundary condition to numerically solve the creeping-flow Stokes equations for the flow of a two-dimensional slab of fluid surrounded by a no-slip, moving boundary (61). This method effectively interpolates the velocity of the cell's deforming boundary to give the associated fluid velocity within the bulk of the cytoplasm.

The Stokes flow solution based on the moving cell boundary is illustrated for an example snapshot in Fig. 2 *c*. We compared this computed flow field with trajectories of lysosome particles that had been smoothed over time and space, as described in Materials and Methods. On average, an $86 \pm 4\%$ correlation was found between the measured particle velocities and the calculated flow field. When velocity is calculated relative to the cell frame of reference, so that only the deformation and not the overall translational motion of the cell is included, a $58 \pm 2\%$ correlation with measured lysosome motion is still observed.

The calculated fluid flow based on the cell's deformation was used to simulate the motion of point particles embedded in the flow (Fig. 2 *d*), with and without an additional diffusive component to their motion. The interparticle MSD of these simulated tracer particles matched both the scaling and the overall magnitude of lysosomes tracked in a large number of crawling HL60 cells (Fig. 3). A comparison of the relative

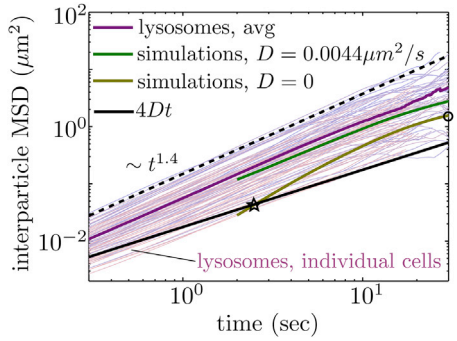

FIGURE 3 Interparticle MSD for particles in a deforming cell. Time and ensemble averages for lysosomes tracked in individual cells are shown as thin curves, with the average for all cells shown in the top thick curve. Central and bottom thick curves show interparticle MSD for simulated particles with and without diffusion, respectively. The thick black line gives expected MSD for diffusive motion alone. The circled point indicates the values used for calculating effective Péclet number ($\mathrm{Pe_{eff}}$). The starred point indicates the time where motion due to fluid flow begins to dominate over purely diffusive motion for simulated particles. To see this figure in color, go online.

effects of deformation-driven flow versus diffusion showed that the simulated cytoplasmic flow dominates at times above $\sim$3 s (Fig. 3). These timescales are highly relevant for the biological function of these cells, which engage in prolific phagocytosis, transporting vesicles to and from the cell periphery over the course of 10 s timescales (62).

We note that because the cell outline was interpolated from intermittent phase images at 4 s time intervals, the calculated flow at shorter time intervals is more persistent than one would expect for actual flows in the cell. Although we cannot resolve them in our experimental setup, cell boundary fluctuations due to thermal noise and active forces generated by membrane-associated proteins are expected to contribute on shorter timescales. In particular, ATP-driven fluctuations of red blood cell membranes have been found to dominate membrane motion above 0.1 s (63,64), and fluctuations due the active transitions of membrane channels may arise at millisecond timescales (65). The advective flows engendered by such fluctuations could contribute to the superdiffusive $t^{1.4}$ scaling of particle motion that continues below subsecond times. Nevertheless, our results indicate the important contribution of deformation-driven fluid flow to particle motion above timescales of a few seconds.

The relative importance of advective versus diffusive transport for a set of particles is generally characterized by the Péclet number, defined as the ratio of times required for a particle to traverse a relevant length scale by fluid flow versus by diffusion (61). The instantaneous particle velocities relative to the cell frame of reference (smoothed over 1 s time intervals to remove the diffusive component) were found to have an average magnitude of $\langle |\vec{v}|_{\mathrm{rms}} \rangle \approx 0.2\ \mu$m/s. However, due to the time-varying direction of the particle motion as the cell deforms, these instantaneous velocities do not translate directly into the

time required for particles to traverse distances of several microns. Instead, we account for the time-varying nature of the flow by defining an effective Péclet number, $\mathrm{Pe}_{\mathrm{eff}} = L_{\mathrm{flow}}^2/(D\Delta t)$, comparing the distance traveled by particles via advective flow (L_{flow}) versus diffusion over a timescale, Δt. The diffusion coefficient of lysosomal particles in HL60 cells has been previously measured as 0.0044 μm^2/s (43). Using $\Delta t = 30$s and $L_{\mathrm{flow}}^2 = 1.5\ \mu$m^2, based on our simulations of deformation-driven flow alone (Fig. 3), gives an effective Péclet number of $\mathrm{Pe}_{\mathrm{eff}} = 11$. A Péclet number substantially above unity indicates a transport process where flow dominates over diffusion. We note that this dimensionless quantity is expected to scale linearly with the radius of the particle. Thus, although the cytoplasmic flow contributes greatly to the motion of lysosomes (radius of $0.2 - 0.5\ \mu$m), it is expected to have a much smaller effect on molecular complexes sized in the tens of nanometers.

The above Péclet number calculations emphasize the importance of the cytoplasmic fluid flow for vesicle motion on timescales of $1 - 30$s. These timescales, however, are still short compared to the time required for a cell to catch and phagocytose a pathogen, as well as the time for a passive (purely diffusing) particle to cover the full extent of the cell (10 μm). Our experimental imaging setup limits the length of time over which individual particles can be tracked before photobleaching or going out of focus. We therefore proceed to a more abstract description of the deformation-driven fluid flow, using a simplified in silico model that enables us to explore the effects of this phenomenon at longer timescales.

Computational model for deformation-driven flow

The results on the importance of cytoplasmic fluid flow in neutrophil-like cells inspire a more general physical question: to what extent does deformation of the boundary of a fluid domain affect the mixing of embedded diffusing particles? We explore this question numerically, using the simplest possible model for domain deformation that reproduces essential features of motile cell behavior. Although our experimental system confined neutrophils to a two-dimensional environment, these cells deform in three dimensions when crawling within human tissue, and we therefore consider particle motion in both two- and three-dimensional deforming fluid domains.

We focus on quasi-spherical domains, filled with an incompressible highly viscous fluid, which undergo periodic extension with period τ. The cytoplasm is a low Reynolds number environment (66), so that the motion of the fluid can be described by the Stokes creeping-flow equations (61). A periodic deformation of our domain along a defined axis will slightly enhance particle diffusivity due to Taylor dispersion (Fig. S2), and can speed up encounters to different cellular structures simply by bringing regions of the cell boundary in temporarily close proximity (discussed below). However, we recall the famous scallop theorem (58), which states that any time-reversible deformation in a fluid at high Reynold's number will lead to no net motion. We would thus expect such a constant-axis deformation to be missing a crucial feature that contributes to particle mixing: the Lagrangian chaos that results from unsteady nonreversible flow (44), leading to net motion within the fluid even in the absence of diffusion (Supporting Materials and Methods; Fig. S3).

To include this effect, we incorporate a "kneading," rather than purely periodic extension of the fluid domain, allowing the axis of deformation to vary continuously, rotating with velocity γ in an arbitrary direction that is selected randomly at the start of each deformation period (Fig. 4 *a*). We note that particle distributions are visibly perturbed by this flow after only a few deformation periods

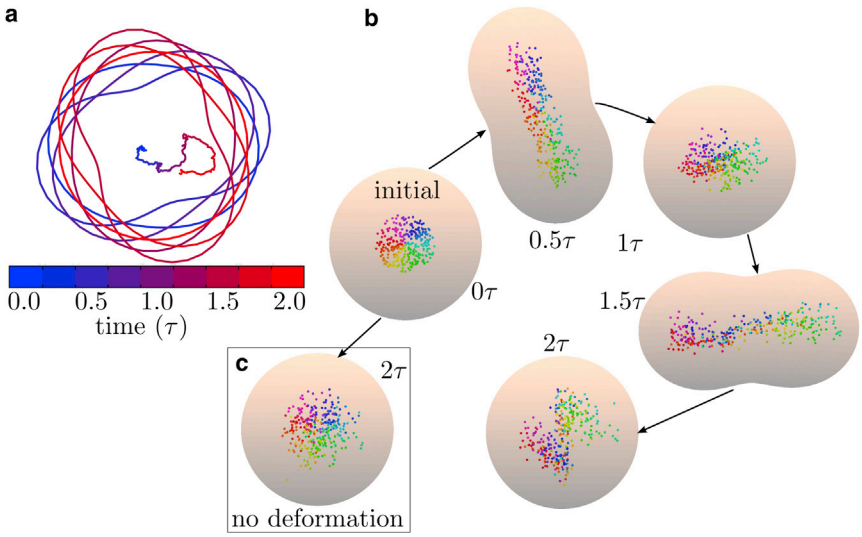

FIGURE 4 Simplified in silico model for particle motion in a deforming fluid domain. (*a*) Deformation of a two-dimensional domain, and example trajectory of an embedded particle driven by diffusion and deformation-associated fluid flow. Times are shown in multiples of the deformation period. (*b*) Snapshots of deforming domain in three dimensions, demonstrating mixing of particles. Particles are colored by initial position. Dimensionless parameters are set to $\widehat{D} = 0.004$, $\widehat{\gamma} = 1.5$. (*c*) Particle mixing by diffusion only, with no domain deformation, is shown for comparison. To see this figure in color, go online.

(Fig. 4, *b* and *c*). This highly simplified description of domain deformation is designed to encompass the fundamental coarse features of morphological dynamics in crawling HL60 cells, obtained from long-time video microscopy of cell behavior (Movies S3 and S4). Namely, these cells tend to polarize and engage in persistent runs over minute-long timescales. During these runs, the direction of their motion (and consequently their axis of elongation) slowly drifts, as represented by the axis rotation in our kneading motion. Runs are terminated when the cells depolymerize and begin to bleb, after which they again polarize and begin to move in an arbitrary new direction (corresponding to elongation along a randomly chosen axis in our model). The extraction of parameters for the kneading dynamics from experimental data is discussed in Supporting Materials and Methods, *Parameter estimation from HL60 trajectory statistics*.

The computational model described here was chosen for its maximal simplicity, with the system behavior governed by very few parameters, all of which can be estimated from experimental data. We nondimensionalize all lengths by the undeformed domain radius R_0, and all times by the deformation period τ. The remaining parameters of interest are the dimensionless particle diffusivity $\widehat{D} = D\tau/R_0^2$ and the dimensionless angular rate of axis drift $\widehat{\gamma} = \gamma\tau$. An additional parameter governing the maximal elongation is set to give an aspect ratio of 2 and is kept constant throughout. Based on statistical analysis of long-time whole-cell trajectories, we estimate the relevant parameters for lysosome motion in HL60 cells to be $\widehat{D} \approx 0.007$ and $\widehat{\gamma} \approx 1.1$, as described in Supporting Materials and Methods, *Parameter estimation from HL60 trajectory statistics*.

We numerically simulate the fluid flow in such a deforming quasi-spherical domain, in both two and three dimensions, using a spectral boundary integral method (67) (Supporting Materials and Methods, *Simulating flow in a deforming domain with the spectral boundary integral method*). The Lagrangian motion of diffusing particles within this domain is tracked over time. The resulting interparticle MSD is comparable in magnitude and scaling to that measured for lysosomes within crawling HL60 cells (Fig. S4), supporting the relevance of this highly simplified model for describing in vivo particle motion.

We note that since our simplified model introduces a single, well-defined timescale for correlations of the fluid flow (the deformation period τ), we do not expect it to yield a consistent polynomial scaling for the MSD versus time. Instead we would expect a transition in scaling behavior before and after τ, as the system transitions from being driven by an effectively constant flow at short times to a random flow at times much longer than the deformation period. Specifically, the particle motion should switch from a diffusive scaling at short times to a ballistic scaling on timescales where the persistent flow velocity dominates over diffusion ($\widehat{D}\tau \ll t \ll \tau/2$), followed by diffusive scaling again at times far above $\tau/2$ as the direction of flow itself is randomized. The latter regime is never reached due to particle confinement within the finite domain. For the parameters used to model lysosome motion in neutrophils ($\widehat{D}\tau \approx 1$ s), the observed timescales (0.3–30 s) fall within the transition range between diffusive behavior and flow coupled with geometric confinement, yielding apparent superdiffusive yet subballistic scaling (Fig. S4). A true superdiffusive power-law scaling of the MSD would require shape fluctuations over a wide range of shorter timescales, which can be achieved by a variety of active processes in the cell (63,65), but which are not resolvable given our current experimental setup. We thus employ our simplified model to focus on the effect of slow whole-cell deformation on particle motion and mixing over the second to minute timescales.

Encounter kinetics in a deforming fluid domain

Using the computational model for particle motion in a simplified deforming domain, we set out to quantify the extent to which the fluid flow arising from domain deformation enhances the mixing of embedded particles. A number of different metrics have been developed for characterizing particle mixing, including ones that track the approach of a bolus of particles toward uniform spread (68), and ones that quantify the mixing of two different classes of particles that are initially separated (69,70). We focus here on a quantitative metric that is of particular relevance to cell physiology, namely, the rate at which particles beginning in the central region of the domain first encounter the domain boundary. This metric serves as an approximation for the passive rate of transit by which particles generated near the cell nucleus encounter the cell membrane during exocytosis or export of membrane-associated proteins.

In particular, we initiate simulations with a group of particles uniformly distributed within a sphere of radius $0.4R_0$ at the center of the domain. We then track over time the number of particles that come within an absorbing distance $0.02R_0$ of the domain boundary. Absorbed particles are removed from the simulation, so that only the first encounter time is recorded. For the case of slow particle diffusion, the simulation time required to run until all of the particles have been absorbed is prohibitively long. Instead, we focus on the cumulative distribution of absorption times up to a maximum time of 20 deformation periods (Fig. 5 *a*). This distribution is fit to the functional form expected for first passage times within an undeformed absorbing sphere, and the fitted effective diffusion coefficient D_{eff} is then calculated for each individual simulation of several thousand particles (see Supporting Materials and Methods, *Fitting D_{eff} for boundary encounter rates*). For each value of particle diffusivity $\widehat{D}$ and axis motion $\widehat{\gamma}$, the results are averaged over 10 simulation replicates, which randomize the initial axis and direction of axis rotation at each

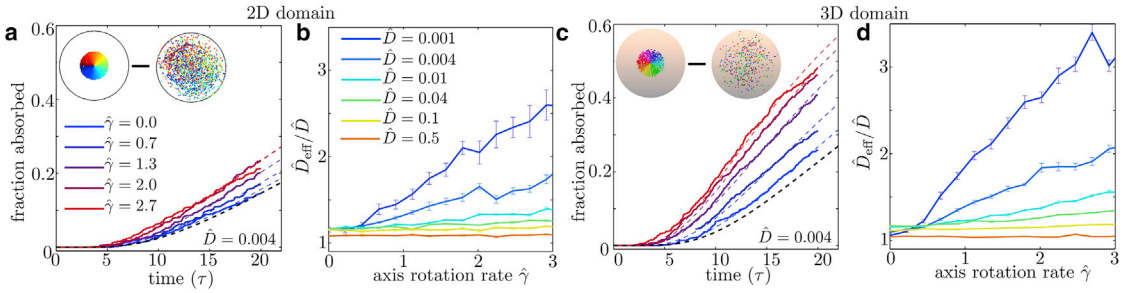

FIGURE 5 Effect of deformation-driven flow on rate of encounter to cell periphery. (*a*) For two-dimensional simulations with particle diffusivity $\widehat{D} = 0.004$, the cumulative fraction of particles that arrive at the outer boundary is plotted versus nondimensionalized time. Dashed lines indicate fits to analytical solution for diffusion in a spherical domain (Supporting Materials and Methods, *Fitting D_{eff} for boundary encounter rates*), with effective diffusivity $\widehat{D}_{\rm eff}$ allowed to vary. The black dashed line gives exact solution with no domain deformation ($\widehat{D}_{\rm eff} = \widehat{D}$). The inset shows initial and final particle distributions. (*b*) Fitted effective diffusivity is plotted as a function of axis rotation rate $\widehat{\gamma}$, for different values of particle diffusivity. The ratio $D_{\rm eff}/D$ indicates the relative extent to which particle encounter is accelerated by domain deformation. Results for each set of parameters are averaged over 10 simulation replicates. (*c* and *d*) Equivalent plots for three-dimensional simulations. To see this figure in color, go online.

deformation period. The simulations are carried out for both two- and three-dimensional domains (Fig. 5, *c* and *d*), with a greater enhancement in encounter rates observed for three-dimensional flows.

As expected, the greatest enhancement in particle encounter to the domain boundary occurs at low diffusivity and high rate of axis rotation. The dimensionless diffusion coefficient $\widehat{D}$ is nondimensionalized by the domain size and deformation period, so that $\widehat{D} = 0.5$ corresponds to rapidly diffusing particles whose mean-squared radial displacement in one deformation period equals the domain size. In this case, no additional enhancement in particle transport is achieved from the deformation-driven flow because particles on average hit the domain boundary at timescales too small for the flow to become significant. For small rates of axis rotation $\widehat{\gamma} \to 0$, the effect of mixing due to nonreversible flow disappears, and very small enhancements in encounter rates are observed. For the values relevant to vesicle motion in neutrophils ($\widehat{D} = 0.007, \widehat{\gamma} \approx 1.1$), however, the rates of boundary encounter (as measured by $D_{\rm eff}$) are enhanced by $\sim$30%. We note that the enhancement in particle encounters is greater in the three-dimensional than in the two-dimensional case, as is to be expected given that consecutive deformation periods in two dimensions with opposite directions of axis rotation tend to unwind the flow-stretched distributions of particles (Fig. S3).

In addition to the rate of encounter at the outer boundary, a metric of equal interest is the rate at which particles starting near the outer boundary of the domain encounter the cell nucleus. The transit of vesicles from the cell periphery to the center is of relevance both for endocytosis of foreign particles (a prominent function of neutrophil cells) and for the transport of membrane-associated signaling molecules into the bulk of the cell. From a physical perspective, the presence of the nucleus raises an interesting complication to the fluid flow. Because the outer boundary of an HL60 cell deforms as it crawls, the nucleus remains relatively unperturbed in its size and shape (Movie S4). The nucleus does rotate substantially in the laboratory frame of reference. However, given the highly simplified nature of our abstract model for domain boundary deformation, we assume the same periodically extending and kneading motion in the reference frame of the nucleus itself. In our model, we thus treat the nucleus as a stationary central sphere with a no-slip boundary and calculate the deformation-driven fluid flow accordingly. The rate of encounter for simulated particles that begin at the periphery to first approach the solid central region (Fig. 6) shows similar trends to those observed for the outer boundary encounter, with an enhancement of $\sim$40% for parameter values relevant to vesicle motion in neutrophils. Unlike the results of Fig. 5, a notable enhancement in encounter rates is observed even with constant axis deformation. This effect arises due to the deformation itself, which brings the outer boundary and its nearby particles in close proximity to the undeformed nucleus, and is seen even in the case of constant

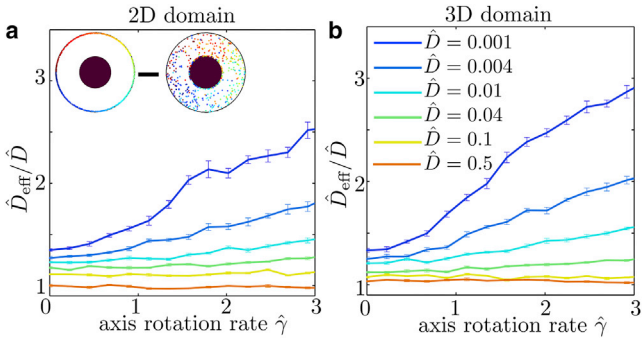

FIGURE 6 Effect of deformation-driven flow on rate of encounter to central frozen region. (*a*) Effective diffusivity obtained by fitting cumulative encounter time distributions to analytical solution for undeformed domain (Supporting Materials and Methods, *Fitting D_{eff} for boundary encounter rates*), plotted for two-dimensional simulations, averaged over 10 replicates each. Inset shows start and end particle distributions for an example simulation, with central frozen region shown in purple. (*b*) Effective diffusivity for three-dimensional deforming domain, fitted to corresponding analytical solution. To see this figure in color, go online.

axis deformation. An analogous effect is observed for the rate with which particles near the center encounter the outer boundary in the presence of a solid nucleus. Here, again, the encounter rate is enhanced for slowly diffusing particles even in the absence of axis rotation (Fig. S5).

Our simplified in silico model shows that, in both two and three dimensions, the rate at which particles transition between the cell periphery and the central region can be substantially enhanced by domain deformation and the associated fluid flow. This enhancement is observed on timescales of 10–20 min (Fig. 5, *a* and *c*); too long for individual particles to be experimentally tracked using our current method, but within the range relevant to neutrophil chemotactic motility and processing of phagocytosed prey (71).

CONCLUSIONS

Using a combination of intracellular particle tracking measurements and numerical simulations, we have shown that the cytoplasmic flow associated with cell shape deformation has the potential to contribute significantly to the motion and transport of organelles within motile cells. Focusing on lysosome motion in neutrophil-like HL60 cells, we demonstrated a superdiffusive scaling for the interparticle MSD that is consistent with the cytoplasmic flows that are expected to arise from the observed deformation of the cell boundary. In this cell type, the cell deformation is sufficiently large and sufficiently rapid that the associated fluid flows are expected to dominate over diffusion for vesicle motion on timescales of seconds or longer.

A simplified computational model for particle motion in a deforming quasi-spherical domain was used to address the general physical question of how much such deformation-driven flows contribute to the mixing of embedded particles. In particular, we showed that for parameter regimes relevant to vesicle motion within neutrophils, the deformation contributes substantially to the rate at which particles transition between the cell periphery and a central nucleus. We identify the two main dimensionless parameters that determine the magnitude of this effect: particle diffusivity relative to the size of the domain and the timescale of deformation, as well as the amount by which the deformation axis rotates in one deformation period. The latter parameter is crucial for establishing nonreversible flows that greatly enhance particle mixing.

The ability to transport vesicles between the cell center and periphery is crucial to a large number of cellular functions, including endocytosis and signal processing. Thus, the enhanced transport rates seen here are likely to contribute to important biological processes in the cell. Promising future extensions of this work could focus on the importance of analogous flows in other deforming cell types, such as *Acanthamoeba*, *Dictyostelium*, fibroblasts, and macrophages. Furthermore, our assumption of a purely viscous cytoplasm could be expanded to encompass a time-dependent rheology, with a cytoplasm that transitions from primarily elastic on short timescales to primarily viscous at long timescales. Such an extension would require development of a mechanical model for the constitutive behavior of the cytoplasm across many orders of magnitude in time, marrying together results from active microrheology and bulk rheology experiments. Because viscoelasticity can enhance the mixing of particles under flow (72), extending our results to explore transport in a deforming viscoelastic domain is a promising avenue for future study.

The boundary conditions in our abstract model are purposefully chosen to be as simple as possible to minimize the number of defining parameters. Additional key questions remain regarding the role of the nucleus as an effectively solid inclusion within the viscous or viscoelastic cytoplasm. In particular, active agitation within the cytoplasm is thought to contribute to nucleus motion relative to the outer boundary (73), as well as deformation and possible rupture of the nucleus itself (74,75). Determining how the internal flow is coupled to the deformation and translocation of the nucleus will require the development of a model for the material properties of the nucleus and for the interaction of cytoplasmic forces with the nuclear boundary. The nuclear motion, in turn, is likely to have substantial impact on the movement of cytoplasmic organelles between the cell periphery and the nucleus. Although outside the scope of this work, these extensions form an intriguing possibility for future study.

SUPPORTING MATERIAL

Supporting Materials and Methods, five figures, and four movies are available at http://www.biophysj.org/biophysj/supplemental/S0006-3495(17)31020-2.

AUTHOR CONTRIBUTIONS

E.F.K. designed research, analyzed data, developed computational models, and wrote the article. C.K.C. designed and performed experiments. J.A.T. designed research and wrote the article.

ACKNOWLEDGMENTS

We are grateful to Eric Shaqfeh, Vivek Narsimhan, and Alexander Groisman for helpful discussions, as well as to Hong Zhao for providing example code.

E.F.K. was supported by the James S. McDonnell Foundation postdoctoral fellowship award in Complex Systems. C.K.C. was supported by the Stanford Cellular and Molecular Biology training grant (T32-GM007276). J.A.T. was funded by the Howard Hughes Medical Institute and the Stanford Center for Systems Biology (P50-GM107615).

REFERENCES

1. Hirokawa, N., Y. Noda, …, S. Niwa. 2009. Kinesin superfamily motor proteins and intracellular transport. *Nat. Rev. Mol. Cell Biol.* 10:682–696.

2. Fakhri, N., A. D. Wessel, …, C. F. Schmidt. 2014. High-resolution mapping of intracellular fluctuations using carbon nanotubes. *Science.* 344:1031–1035.
3. Fodor, É., W. W. Ahmed, …, F. van Wijland. 2016. Nonequilibrium dissipation in living oocytes. *Europhys. Lett.* 116:30008.
4. Brangwynne, C. P., G. H. Koenderink, …, D. A. Weitz. 2009. Intracellular transport by active diffusion. *Trends Cell Biol.* 19:423–427.
5. Guo, M., A. J. Ehrlicher, …, D. A. Weitz. 2014. Probing the stochastic, motor-driven properties of the cytoplasm using force spectrum microscopy. *Cell.* 158:822–832.
6. Lin, C., M. Schuster, …, G. Steinberg. 2016. Active diffusion and microtubule-based transport oppose myosin forces to position organelles in cells. *Nat. Commun.* 7:11814.
7. van de Meent, J.-W., A. J. Sederman, …, R. E. Goldstein. 2010. Measurement of cytoplasmic streaming in single plant cells by magnetic resonance velocimetry. *J. Fluid Mech.* 642:5–14.
8. Ganguly, S., L. S. Williams, …, R. E. Goldstein. 2012. Cytoplasmic streaming in Drosophila oocytes varies with kinesin activity and correlates with the microtubule cytoskeleton architecture. *Proc. Natl. Acad. Sci. USA.* 109:15109–15114.
9. Niwayama, R., H. Nagao, …, A. Kimura. 2016. Bayesian inference of forces causing cytoplasmic streaming in caenorhabditis elegans embryos and mouse oocytes. *PLoS One.* 11:e0159917.
10. Keren, K., P. T. Yam, …, J. A. Theriot. 2009. Intracellular fluid flow in rapidly moving cells. *Nat. Cell Biol.* 11:1219–1224.
11. Maître, J.-L., R. Niwayama, …, T. Hiiragi. 2015. Pulsatile cell-autonomous contractility drives compaction in the mouse embryo. *Nat. Cell Biol.* 17:849–855.
12. Lewis, O. L., S. Zhang, …, J. C. del Álamo. 2015. Coordination of contractility, adhesion and flow in migrating Physarum amoebae. *J. R. Soc. Interface.* 12:20141359.
13. Alim, K., G. Amselem, …, A. Pringle. 2013. Random network peristalsis in Physarum polycephalum organizes fluid flows across an individual. *Proc. Natl. Acad. Sci. USA.* 110:13306–13311.
14. Reverey, J. F., J.-H. Jeon, …, C. Selhuber-Unkel. 2015. Superdiffusion dominates intracellular particle motion in the supercrowded cytoplasm of pathogenic Acanthamoeba castellanii. *Sci. Rep.* 5:11690.
15. Felder, S., and E. L. Elson. 1990. Mechanics of fibroblast locomotion: quantitative analysis of forces and motions at the leading lamellas of fibroblasts. *J. Cell Biol.* 111:2513–2526.
16. Felder, S., and Z. Kam. 1994. Human neutrophil motility: time-dependent three-dimensional shape and granule diffusion. *Cell Motil. Cytoskeleton.* 28:285–302.
17. Charras, G. T., M. Coughlin, …, L. Mahadevan. 2008. Life and times of a cellular bleb. *Biophys. J.* 94:1836–1853.
18. Charras, G., and E. Paluch. 2008. Blebs lead the way: how to migrate without lamellipodia. *Nat. Rev. Mol. Cell Biol.* 9:730–736.
19. Mills, J. C., N. L. Stone, …, R. N. Pittman. 1998. Apoptotic membrane blebbing is regulated by myosin light chain phosphorylation. *J. Cell Biol.* 140:627–636.
20. Charras, G. T., J. C. Yarrow, …, T. J. Mitchison. 2005. Non-equilibration of hydrostatic pressure in blebbing cells. *Nature.* 435:365–369.
21. Mitchison, T., G. Charras, and L. Mahadevan. 2008. Implications of a poroelastic cytoplasm for the dynamics of animal cell shape. *Semin. Cell Dev. Biol.* 19:215–223.
22. Wirtz, D. 2009. Particle-tracking microrheology of living cells: principles and applications. *Annu. Rev. Biophys.* 38:301–326.
23. Gal, N., D. Lechtman-Goldstein, and D. Weihs. 2013. Particle tracking in living cells: a review of the mean square displacement method and beyond. *Rheol. Acta.* 52:425–443.
24. Chevry, L., R. Colin, …, J.-F. Berret. 2013. Intracellular microrheology probed by micron-sized wires. *Biomaterials.* 34:6299–6305.
25. Arcizet, D., B. Meier, …, D. Heinrich. 2008. Temporal analysis of active and passive transport in living cells. *Phys. Rev. Lett.* 101:248103.
26. Yamada, S., D. Wirtz, and S. C. Kuo. 2000. Mechanics of living cells measured by laser tracking microrheology. *Biophys. J.* 78:1736–1747.
27. Tolić-Nørrelykke, I. M., E.-L. Munteanu, …, K. Berg-Sørensen. 2004. Anomalous diffusion in living yeast cells. *Phys. Rev. Lett.* 93:078102.
28. Berret, J.-F. 2016. Local viscoelasticity of living cells measured by rotational magnetic spectroscopy. *Nat. Commun.* 7:10134.
29. Wilhelm, C. 2008. Out-of-equilibrium microrheology inside living cells. *Phys. Rev. Lett.* 101:028101.
30. Almonacid, M., W. W. Ahmed, …, M.-H. Verlhac. 2015. Active diffusion positions the nucleus in mouse oocytes. *Nat. Cell Biol.* 17:470–479.
31. Fodor, É., M. Guo, …, F. van Wijland. 2015. Activity-driven fluctuations in living cells. *Europhys. Lett.* 110:48005.
32. Katrukha, E. A., M. Mikhaylova, …, L. C. Kapitein. 2017. Probing cytoskeletal modulation of passive and active intracellular dynamics using nanobody-functionalized quantum dots. *Nat. Commun.* 8:14772.
33. Trepat, X., G. Lenormand, and J. J. Fredberg. 2008. Universality in cell mechanics. *Soft Matter.* 4:1750.
34. Ahmed, W. W., É. Fodor, and T. Betz. 2015. Active cell mechanics: measurement and theory. *Biochimica et Biophysica Acta.* 1853:3083–3094.
35. Gupta, S. K., and M. Guo. 2017. Equilibrium and out-of-equilibrium mechanics of living mammalian cytoplasm. *J. Mech. Phys. Solids.* 107:284–293.
36. Fardin, M. A., O. M. Rossier, …, M. P. Sheetz. 2010. Cell spreading as a hydrodynamic process. *Soft Matter.* 6:4788–4799.
37. Orly, G., M. Naoz, and N. S. Gov. 2014. Physical model for the geometry of actin-based cellular protrusions. *Biophys. J.* 107:576–587.
38. Callan-Jones, A. C., V. Ruprecht, …, R. Voituriez. 2016. Cortical flow-driven shapes of nonadherent cells. *Phys. Rev. Lett.* 116:028102.
39. Copos, C. A., S. Walcott, …, R. D. Guy. 2017. Mechanosensitive adhesion explains stepping motility in amoeboid cells. *Biophys. J.* 112:2672–2682.
40. Theriot, J. A., and T. J. Mitchison. 1991. Actin microfilament dynamics in locomoting cells. *Nature.* 352:126–131.
41. Fritzsche, M., A. Lewalle, …, G. Charras. 2013. Analysis of turnover dynamics of the submembranous actin cortex. *Mol. Biol. Cell.* 24:757–767.
42. Hochmuth, R. M. 2000. Micropipette aspiration of living cells. *J. Biomech.* 33:15–22.
43. Koslover, E. F., C. K. Chan, and J. A. Theriot. 2016. Disentangling random motion and flow in a complex medium. *Biophys. J.* 110:700–709.
44. Chaiken, J., R. Chevray, …, Q. M. Tan. 1986. Experimental study of Lagrangian turbulence in a Stokes flow. *Proc. R. Soc. Lond. Ser. A.* 408:165–174.
45. Ottino, J. M. 1989. The Kinematics of Mixing: Stretching, Chaos, and TransportVol. 3. Cambridge University Press, Cambridge, United Kingdom.
46. Chaiken, J., C. K. Chu, …, Q. M. Tan. 1987. Lagrangian turbulence and spatial complexity in a Stokes flow. *Phys. Fluids.* 30:687.
47. Aref, H., and S. Balachandar. 1986. Chaotic advection in Stokes flow. *Phys. Fluids.* 29:3515–3521.
48. Jansons, K. M. 2006. On Taylor dispersion in oscillatory channel flows. *Proc. Math. Phys. Eng. Sci.* 462:3501–3509.
49. Crocker, J. C., and D. G. Grier. 1996. Methods of digital video microscopy for colloidal studies. *J. Colloid Interface Sci.* 179:298–310.
50. Crocker, J. C., and B. D. Hoffman. 2007. Multiple-particle tracking and two-point microrheology in cells. *Methods Cell Biol.* 83:141–178.
51. Wilson, C. A., and J. A. Theriot. 2006. A correlation-based approach to calculate rotation and translation of moving cells. *IEEE Trans. Image Process.* 15:1939–1951.

52. Lucas, J. S., Y. Zhang, …, C. Murre. 2014. 3D trajectories adopted by coding and regulatory DNA elements: first-passage times for genomic interactions. *Cell.* 158:339–352.

53. Vazquez, J., A. S. Belmont, and J. W. Sedat. 2001. Multiple regimes of constrained chromosome motion are regulated in the interphase Drosophila nucleus. *Curr. Biol.* 11:1227–1239.

54. Seroussi, I., D. Veikherman, …, K. Keren. 2012. Segmentation and tracking of live cells in phase-contrast images using directional gradient vector flow for snakes. *J. Microsc.* 247:137–146.

55. Goldstein, D., T. Elhanan, …, D. Weihs. 2013. Origin of active transport in breast-cancer cells. *Soft Matter.* 9:7167–7173.

56. Hendricks, A. G., E. Perlson, …, E. L. Holzbaur. 2010. Motor coordination via a tug-of-war mechanism drives bidirectional vesicle transport. *Curr. Biol.* 20:697–702.

57. Bálint, Š., I. V. Vilanova, …, M. Lakadamyali. 2013. Correlative live-cell and superresolution microscopy reveals cargo transport dynamics at microtubule intersections. *Proc. Natl. Acad. Sci. USA.* 110:3375–3380.

58. Purcell, E. M. 1977. Life at low Reynolds number. *Am. J. Phys.* 45:3.

59. Lee, J., M. Gustafsson, …, K. Jacobson. 1990. The direction of membrane lipid flow in locomoting polymorphonuclear leukocytes. *Science.* 247:1229–1233.

60. Kucik, D. F., E. L. Elson, and M. P. Sheetz. 1990. Cell migration does not produce membrane flow. *J. Cell Biol.* 111:1617–1622.

61. Leal, L. G. 2007. Advanced Transport Phenomena: Fluid Mechanics and Convective Transport Processes. Cambridge University Press, Cambridge, United Kingdom.

62. Kikushima, K., S. Kita, and H. Higuchi. 2013. A non-invasive imaging for the in vivo tracking of high-speed vesicle transport in mouse neutrophils. *Sci. Rep.* 3:1913.

63. Betz, T., M. Lenz, …, C. Sykes. 2009. ATP-dependent mechanics of red blood cells. *Proc. Natl. Acad. Sci. USA.* 106:15320–15325.

64. Turlier, H., D. A. Fedosov, …, T. Betz. 2016. Equilibrium physics breakdown reveals the active nature of red blood cell flickering. *Nat. Phys.* 12:513–519.

65. Gov, N. 2004. Membrane undulations driven by force fluctuations of active proteins. *Phys. Rev. Lett.* 93:268104.

66. Berg, H. C. 1993. Random Walks in Biology. Princeton University Press, Princeton, New Jersey.

67. Zhao, H., and E. S. Shaqfeh. 2011. The dynamics of a vesicle in simple shear flow. *J. Fluid Mech.* 674:578–604.

68. Ashwin, P., M. Nicol, and N. Kirkby. 2002. Acceleration of one-dimensional mixing by discontinuous mappings. *Physica A.* 310:347–363.

69. Danckwerts, P. 1952. The definition and measurement of some characteristics of mixtures. *Appl. Sci. Res.* 3:279–296.

70. Camesasca, M., M. Kaufman, and I. Manas-Zloczower. 2006. Quantifying fluid mixing with the Shannon entropy. *Macromol. Theory Simul.* 15:595–607.

71. Colucci-Guyon, E., J.-Y. Tinevez, …, P. Herbomel. 2011. Strategies of professional phagocytes in vivo: unlike macrophages, neutrophils engulf only surface-associated microbes. *J. Cell Sci.* 124:3053–3059.

72. Groisman, A., and V. Steinberg. 2000. Elastic turbulence in a polymer solution flow. *Nature.* 405:53–55.

73. Rupprecht, J.-F., A. Singh, …, J. Prost. 2017. Maximal fluctuations of confined actomyosin gels: dynamics of the cell nucleus. arXiv, arXiv:1703.04395, https://arxiv.org/abs/1703.04395.

74. Thiam, H.-R., P. Vargas, …, M. Piel. 2016. Perinuclear Arp2/3-driven actin polymerization enables nuclear deformation to facilitate cell migration through complex environments. *Nat. Commun.* 7:10997.

75. Denais, C. M., R. M. Gilbert, …, J. Lammerding. 2016. Nuclear envelope rupture and repair during cancer cell migration. *Science.* 352:353–358.